

Spirals and heteroclinic cycles in a spatially extended Rock–Paper–Scissors model of cyclic dominance

C. M. Postlethwaite

Department of Mathematics, Auckland University, Auckland, NZ

A. M. Rucklidge

School of Mathematics, University of Leeds, Leeds LS2 9JT, UK

(Dated: November 11, 2018)

Spatially extended versions of the cyclic-dominance Rock–Paper–Scissors model have traveling wave (in one dimension) and spiral (in two dimensions) behavior. The far field of the spirals behave like traveling waves, which themselves have profiles reminiscent of heteroclinic cycles. We compute numerically a nonlinear dispersion relation between the wavelength and wavespeed of the traveling waves, and, together with insight from heteroclinic bifurcation theory and further numerical results from 2D simulations, we are able to make predictions about the overall structure and stability of spiral waves in 2D cyclic dominance models.

Cyclic dominance has been invoked in recent years as a mechanism for explaining the persistence of biodiversity in nature [1, 2]: examples include microbial organisms [3] and side-blotched lizards [4]. In a well mixed population, one species eventually dominates [5], but persistence of all species is possible when their spatial distribution and mobility is taken into account [1].

The basic processes of growth and cyclic dominance between three species can be modelled as [6]:

$$A + \phi \xrightarrow{1} A + A, \quad A + B \xrightarrow{\sigma} \phi + B, \quad A + B \xrightarrow{\zeta} B + B, \quad (1)$$

where A and B are two of the three species and ϕ represents space for growth, with growth rate 1. Species B dominates A either by removing it (at rate $\sigma \geq 0$) or by replacing it (at rate $\zeta \geq 0$). Processes for the other pairs of species are found by symmetry. Individuals are placed on a spatial lattice and allowed to move to adjacent lattice sites; each lattice site has a carrying capacity N . Mean field equations can then be derived [6, 7]:

$$\begin{aligned} \dot{a} &= a(1 - \rho - (\sigma + \zeta)b + \zeta c) + \nabla^2 a, \\ \dot{b} &= b(1 - \rho - (\sigma + \zeta)c + \zeta a) + \nabla^2 b, \\ \dot{c} &= c(1 - \rho - (\sigma + \zeta)a + \zeta b) + \nabla^2 c, \end{aligned} \quad (2)$$

where (a, b, c) are non-negative functions of space (x, y) and time t , representing the proportions of N of each of the three species, and $\rho = a + b + c$. The coefficient of the diffusion terms is set to 1 by scaling x and y , and nonlinear diffusion effects [8] are suppressed. These equations accurately reproduce stochastic simulations of (1) provided N is large [7].

Without diffusion, (2) has been well studied [9]. It has five non-negative equilibria: the origin $(0, 0, 0)$, coexistence $\frac{1}{3+\sigma}(1, 1, 1)$, and three on the coordinate axes, $(1, 0, 0)$, $(0, 1, 0)$ and $(0, 0, 1)$. The origin is unstable; the coexistence point has eigenvalues -1 and $\frac{1}{2}(\sigma \pm i\sqrt{3}(\sigma + 2\zeta))/(3 + \sigma)$, and the on-axis equilibria have eigenvalues -1 , ζ and $-(\sigma + \zeta)$. When $\sigma > 0$,

the coexistence point is unstable and trajectories are attracted to a heteroclinic cycle between the on-axis equilibria, approaching each in turn, staying close to each for progressively longer times but never stopping [9–11].

Numerical simulations of (2) in sufficiently large two-dimensional (2D) domains with periodic boundary conditions show a variety of behaviors as parameters are changed [6, 12]. Stable spiral patterns are readily found (Fig. 1a), in which regions dominated by A (red) are invaded by B (green), only to be invaded by C (blue). Comparing a cut through the core (Fig. 1b) with a one-dimensional (1D) solution with the same wavelength (Fig. 1c) demonstrates how the behavior far from the core is essentially a 1D traveling wave (TW). Stable 1D TWs can be found with arbitrarily long wavelength (Fig. 1d,e), where (apart from being periodic) the behavior closely resembles a heteroclinic cycle, with traveling fronts between regions where one variable is close to 1 and the others are close to 0.

The question that we ask is: can ideas from nonlinear dynamics and heteroclinic cycles be used to analyze the properties (wavelength, wavespeed and stability) of the 1D TWs and 2D spirals? The approach we take is to consider the 1D TWs as periodic orbits in a moving frame of reference, and use continuation techniques to calculate a nonlinear relationship between the wavelength and wavespeed. We find parameter ranges in which these 1D TWs exist (between a Hopf bifurcation and three different types of heteroclinic bifurcation) and obtain partial information about their stability. The locations of the heteroclinic bifurcations are computed numerically, but in two of the three cases they coincide with straight-forward relationships between eigenvalues. We investigate 2D solutions of the partial differential equations (PDEs) (2) over a range of parameter values, and show numerically that the rotation frequency of the spiral is related to the imaginary part of the eigenvalues of the coexistence fixed point. Combining all this information is enough to determine the overall properties of the spiral.

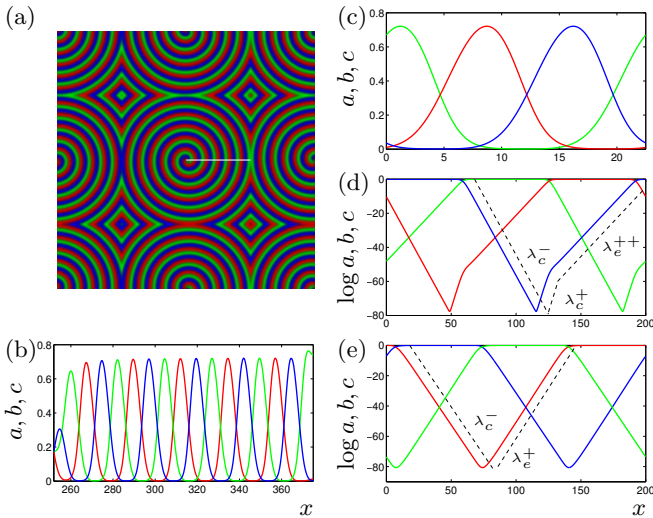


FIG. 1. Numerical solutions of equations (2), with parameters $\sigma = 3.2$, $\zeta = 0.8$ except in (d,e); a , b and c are shown in red, green and blue respectively. Panels (a) and (b) show results from integration in 2D, with domain size 500×500 ; the spiral waves have estimated rotation frequency $\Omega = 0.440$ and far-field wavespeed $\gamma = 1.576$ and wavelength $\Lambda = 22.5$. Panel (b) shows the profile along the white line in (a). Panels (c)–(e) show results from integrations in 1D. In (c), the box size is $\Lambda = 22.5$ (c.f. the waves in (b)). Panel (d) is for a larger box ($\Lambda = 200$), and $\zeta = 0.2$; the profile is shown in log coordinates: a kink (change in slope) is evident in the upward phase of each curve. The estimated wavespeed is $\gamma = 1.059$. Panel (e) has $\zeta = 2$, and a profile without a kink. The estimated wavespeed is $\gamma = 2.834$. The dashed lines in (d) and (e) show slopes as indicated, labelled with eigenvalues from Table I.

We first consider equations (2) in 1D, and move to a traveling frame moving with wavespeed $\gamma > 0$. We define $\xi = x + \gamma t$, then $\frac{\partial}{\partial x} \rightarrow \frac{\partial}{\partial \xi}$ and $\frac{\partial}{\partial t} \rightarrow \gamma \frac{\partial}{\partial \xi} + \frac{\partial}{\partial t}$. Traveling wave solutions in the moving frame have $\frac{\partial}{\partial t} = 0$, and so TW solutions of (2) correspond to periodic solutions of the following set of six first-order ODEs:

$$\begin{aligned} a_\xi &= u, & u_\xi &= \gamma u - a(1 - \rho - (\sigma + \zeta)b + \zeta c), \\ b_\xi &= v, & v_\xi &= \gamma v - b(1 - \rho - (\sigma + \zeta)c + \zeta a), \\ c_\xi &= w, & w_\xi &= \gamma w - c(1 - \rho - (\sigma + \zeta)a + \zeta b). \end{aligned} \quad (3)$$

The period of the periodic solution corresponds to the wavelength Λ of the TW, and in numerical simulations of the PDEs in 1D with periodic boundary conditions, the size of the computational box.

Let $\mathbf{x} = (a, u, b, v, c, w)$. The coexistence and on-axis equilibria of the ODEs (3) are $\mathbf{x} = \frac{1}{3+\sigma}(1, 0, 1, 0, 1, 0)$, $(1, 0, 0, 0, 0, 0)$, $(0, 0, 1, 0, 0, 0)$ and $(0, 0, 0, 0, 1, 0)$. We label these equilibria ξ_h , ξ_a , ξ_b and ξ_c and respectively. Following techniques used in the analysis of heteroclinic cycles (see, e.g. [11]), we identify radial, expanding and contracting subspaces. For ξ_a , these are the (a, u) , (b, v) and (c, w) subspaces respectively. The eigenvalues in each subspace are given in table I. The four-dimensional subspace $\{c = w = 0\}$ is invariant under the flow of (3).

Subspace	Eigenvalues
Radial	$\lambda_r^\pm = \frac{1}{2}(\gamma \pm \sqrt{\gamma^2 + 4})$
Contracting	$\lambda_c^\pm = \frac{1}{2}(\gamma \pm \sqrt{\gamma^2 + 4(\sigma + \zeta)})$
Expanding ($\gamma^2 - 4\zeta > 0$)	$\lambda_e^{++} = \frac{1}{2}(\gamma \pm \sqrt{\gamma^2 - 4\zeta})$
Expanding ($\gamma^2 - 4\zeta < 0$)	$\lambda_e^R \pm i\lambda_e^I = \frac{1}{2}(\gamma \pm i\sqrt{4\zeta - \gamma^2})$

TABLE I. Eigenvalues of the on-axis equilibria of (3). The radial and contracting eigenvalues are always real, and satisfy $\lambda_r^- < 0 < \lambda_r^+$ and $\lambda_c^- < 0 < \lambda_c^+$. If $\gamma^2 > 4\zeta$, the expanding eigenvalues are also real, and $\lambda_e^{++} > \lambda_e^+ > 0$. If $\gamma^2 < 4\zeta$, the expanding eigenvalues $\lambda_e^R \pm i\lambda_e^I$ are complex, and $\lambda_e^R > 0$.

Restricted to this subspace, ξ_a has a three-dimensional unstable manifold, and ξ_b has a two-dimensional stable manifold. These manifolds generically intersect, and there is thus a robust heteroclinic connection between ξ_a and ξ_b . By symmetry, we have a robust heteroclinic cycle between ξ_a , ξ_b and ξ_c .

In numerical solutions of the PDEs (2) in large 1D periodic domains of size Λ , these heteroclinic cycles, which have infinite period, are excluded and we find instead periodic solutions that lie close to the heteroclinic cycle. These solutions spend a lot of “time” (a large interval in the ξ variable) close to the equilibria, where the components grow (or decay) exponentially with rates equal to the relevant eigenvalues (see Fig. 1d,e). In large domains the TW profiles are thus determined by their wavelength Λ and these eigenvalues. We find large- Λ TWs with three different profiles; two of which are shown in Fig. 1(d,e). The profile in (d) takes the form:

$$\log a(\xi) = \begin{cases} 0 & 0 \leq \xi \leq \frac{\Lambda}{3} \\ \lambda_c^-(\xi - \frac{\Lambda}{3}) & \frac{\Lambda}{3} < \xi \leq \frac{\Lambda}{3} + l \\ \lambda_c^- l + \lambda_c^+(\xi - \frac{\Lambda}{3} - l) & \frac{\Lambda}{3} + l < \xi \leq \frac{2\Lambda}{3} \\ \log a(\frac{2\Lambda}{3}) + \lambda_e^{++}(\xi - \frac{2\Lambda}{3}) & \frac{2\Lambda}{3} < \xi \leq \Lambda \end{cases}$$

and b and c are cyclic permutations, so $b(\xi) = a(\xi - \frac{\Lambda}{3})$ and $c(\xi) = b(\xi - \frac{\Lambda}{3})$. The amount of “decay” in the contracting phase must match the amount of growth in the expanding phase, and these are both of equal length. In this case, this means that there is a switch from decay to growth during the contracting phase at $\xi = \frac{\Lambda}{3} + l$, where $l = \frac{\Lambda}{3} \frac{\lambda_c^+ + \lambda_e^{++}}{\lambda_c^+ - \lambda_c^-}$ (and $0 < l < \frac{\Lambda}{3}$), and a change in the upwards slope (a kink) at $\xi = \frac{2\Lambda}{3}$. The solution is continuous, periodic and has $\log a(\Lambda) = 0$. We have ignored the “time” taken for jumps between the equilibria (which round the sharp corners of the profile) as these are short compared to Λ , so long as Λ is sufficiently large. Generically, when the expanding eigenvalues are real, we expect solutions leaving a neighbourhood of an equilibrium to do so tangent to the leading expanding eigenvector: i.e., an expansion rate equal to λ_e^+ . The profile observed in Fig. 1(d) is non-generic, and corresponds to an orbit flip, discussed further later. The profile in Fig. 1(e) has no

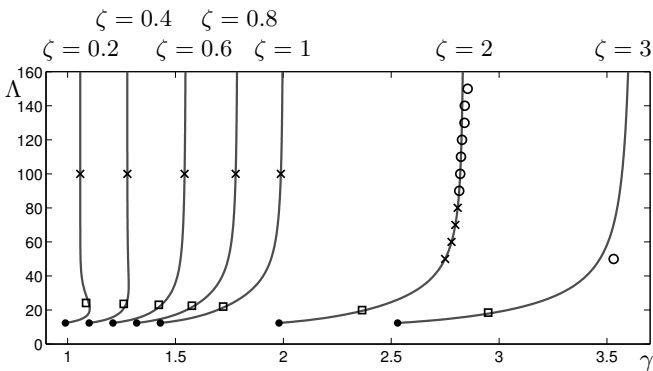


FIG. 2. The wavelength (period) Λ , as γ is varied, of periodic orbits in the ODEs (3), computed using AUTO, with $\sigma = 3.2$ and values of ζ as indicated. Each curve of periodic orbits arises in a Hopf bifurcation on the left (black dot), and is continued numerically until it ends in a heteroclinic (long-period) bifurcation on the right. Effectively these curves are nonlinear dispersion relations for TWs in the PDEs. Symbols indicate the results of 1D TW and 2D spiral solutions of the PDEs (2), as described in the text.

kink, and the rate of expansion is λ_e^+ rather than λ_e^{++} . The third profile observed is similar in shape to that in Fig. 1(d) except that the expanding eigenvalues are very slightly complex.

Although the heteroclinic cycle exists robustly in the ODEs, periodic solutions cannot be found by time-stepping the initial value problem since they are not stable with respect to evolution in the ξ variable. Instead, we identify a Hopf bifurcation at the equilibrium ξ_h , and use the continuation software AUTO [13] to follow periodic orbits, treating the wavespeed γ as a parameter, allowing the wavelength Λ to be adjusted automatically.

The Jacobian matrix at ξ_h has pure imaginary eigenvalues $\pm i\omega_H$ when $\gamma = \gamma_H(\sigma, \zeta)$, where

$$\gamma_H(\sigma, \zeta) \equiv \frac{\sqrt{3}(\sigma + 2\zeta)}{\sqrt{2\sigma(\sigma + 3)}}, \quad \text{and} \quad \omega_H^2 = \frac{\sigma}{2(\sigma + 3)}, \quad (4)$$

at which point a Hopf bifurcation creates periodic orbits of period $\Lambda_H = \frac{2\pi}{\omega_H}$. Fig. 2 shows, for $\sigma = 3.2$ and a range of values of ζ , the wavelength (period) Λ as γ is varied. The range of γ for which periodic solutions can be found depends on σ and ζ ; each branch starts at γ_H and terminates with infinite Λ in a heteroclinic bifurcation.

In Fig. 3 we show a bifurcation diagram (also computed by AUTO) in (γ, ζ) space. Periodic solutions bifurcate to the right of the Hopf bifurcation, given by (4), and disappear in the heteroclinic bifurcation curve (black) on the right. The red and blue curves correspond to simple equalities of the eigenvalues, as indicated in the figure, and divide the parameter space into four labelled regions, defined in table II.

We observe from the numerical results that the heteroclinic bifurcation in Fig. 3 shows three different behaviors, overlying the green, red and blue curves in different

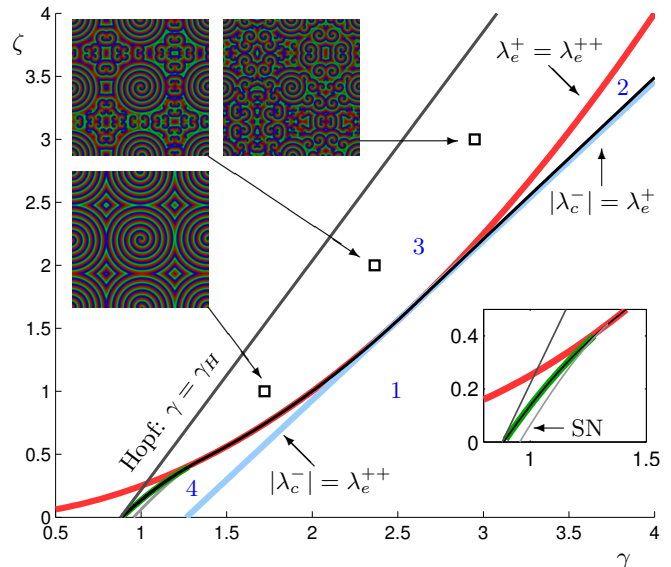


FIG. 3. Bifurcation diagram for the ODEs (3), in (γ, ζ) parameter space, with $\sigma = 3.2$. The blue line ($\zeta = \sqrt{\frac{\sigma}{2}}\gamma - \frac{\sigma}{2}$) and red curve ($4\zeta = \gamma^2$) are tangent at $(\gamma, \zeta) = (\sqrt{2\sigma}, \sigma/2)$ and divide the parameter space into four regions, labeled by blue numbers, and defined in table II. The green curve is the locus of a heteroclinic orbit flip. The dark grey line is a curve of Hopf bifurcations. Periodic orbits bifurcate to the right of this line and disappear in a curve of heteroclinic bifurcations (black). A curve of saddle-node bifurcations of periodic orbits (light grey) exists for smaller ζ . The upper insets show results of 2D simulations at the indicated parameter values. The lower inset is a zoom near the saddle-node (SN) and orbit flip (green) bifurcations.

Region	Definition	Eigenvalue properties
1	$\zeta < \sqrt{\frac{\sigma}{2}}\gamma - \frac{\sigma}{2}$	$\lambda_e^{++} \in \mathbb{R}, \lambda_e^+ < \lambda_c^- < \lambda_e^{++}$
2	$\zeta > \frac{\sigma}{2}, \sqrt{\frac{\sigma}{2}}\gamma - \frac{\sigma}{2} < \zeta < \frac{\gamma^2}{4}$	$\lambda_e^{++} \in \mathbb{R}, \lambda_c^- < \lambda_e^+ < \lambda_e^{++}$
3	$\zeta > \frac{\gamma^2}{4}$	$\lambda_e^{++} \in \mathbb{C}$
4	$\zeta < \frac{\sigma}{2}, \sqrt{\frac{\sigma}{2}}\gamma - \frac{\sigma}{2} < \zeta < \frac{\gamma^2}{4}$	$\lambda_e^{++} \in \mathbb{R}, \lambda_e^+ < \lambda_e^{++} < \lambda_c^- $

TABLE II. Definitions of the regions of parameter space shown in Fig. 3 and eigenvalue properties therein.

parameter regimes, and corresponding to the three long- Λ TW profiles discussed earlier. Before discussing these further, we first note that heteroclinic bifurcations cannot occur in the interiors of regions 2 or 3. In region 2, a large- Λ TW profile would require $l > \frac{\Lambda}{3}$, which cannot occur. In region 3, the expanding eigenvalues are complex. In the large Λ limit, complex eigenvalues are excluded: the invariance of the subspace $\{a = u = 0\}$ means that a cannot change sign along trajectories.

When $\zeta > \frac{\sigma}{2} = 1.6$, the heteroclinic bifurcation occurs on the blue curve, at which point the negative contracting and leading expanding eigenvalues are equal in magnitude, and the TW has an unknicked profile, as in Fig. 1(e). This is a heteroclinic resonance bifurcation [14]. For $0.4 < \zeta < \frac{\sigma}{2} = 1.6$, the heteroclinic bifurcation occurs on

the red curve, at which point the expanding eigenvalues switch from complex to real (a variant of a Belyakov–Devaney bifurcation [15]), and the TW has a kinked profile. For $0 < \zeta < 0.4$, the periodic orbit undergoes a saddle-node bifurcation before the heteroclinic bifurcation; the fold can be seen in the curve for $\zeta = 0.2$ in Fig. 2. In this range of ζ , the heteroclinic bifurcation coincides with an orbit flip bifurcation [16], indicated in green in Fig. 3. The TW has a kinked profile, as in Fig. 1(d). The location of the orbit flip is computed by solving a boundary value problem in the four-dimensional invariant subspace $\{c = w = 0\}$ which requires that the heteroclinic solution is tangent to the λ_e^{++} eigenvector.

Returning to the PDEs (2), we computed solutions over a range of values of σ , ζ and domain size. We imposed periodic boundary conditions, and used Fourier transforms and second-order exponential time differencing [17]. In 2D, we mainly used 1000×1000 domains, with 1536×1536 Fourier modes in each direction. We estimated speeds of TWs (in 1D) and rotation speeds and far-field wavelengths and wavespeeds of spirals (in 2D).

In 1D and with $\sigma = 3.2$, for $\zeta < \frac{\sigma}{2} = 1.6$, we are able to find stable TWs for all box sizes larger than Λ_H . For $\zeta > \frac{\sigma}{2}$, we find that TWs are stable in smaller boxes, and unstable in larger boxes, with a decreasing range of stable box sizes as ζ is increased. For $\zeta = 3$, we are unable to find any stable TWs. The crosses (resp. open circles) on the curves in Fig. 2 show the observed wavespeeds of stable (resp. unstable) TWs for a range of ζ and box sizes. In this context, by “stable” we are referring to how the TWs evolves in time with a fixed wavelength, and we are not considering perturbations that change the wavelength. A full treatment would consider convective and absolute instability of the TWs.

In 2D, spiral waves (or more complex solutions) are usually found if the domain is large enough. We use initial conditions that are one half a and a quarter each b and c , as in [8]. When we find spirals, if they are big enough, we locate the core (where $a = b = c$) and compute the far-field wavelength by looking at a , b and c along a cut through the core, as indicated in Fig. 1(a,b). The period Ω in time is obtained from a timeseries, and the wavespeed estimated as $\gamma = \Lambda/\Omega$. For $\sigma = 3.2$ and for a selection of ζ , we have included in Fig. 3 three examples, along with their (γ, ζ) values, and in Fig. 2 (as open squares) the (γ, Λ) values estimated from spiral solutions. The fact that the open square symbols lie on the continuation curves from AUTO confirms that the far field of the spirals does behave as a 1D TW and obeys the same nonlinear dispersion relation as true 1D solutions.

We now have two relations between three quantities, the rotation frequency Ω of the 2D spiral, and the wavespeed γ and wavelength Λ of the 1D TWs in the far field. The rotation frequency appears to be set by the core, and the far field follows. When locating the core we observed that the common value of the three variables is

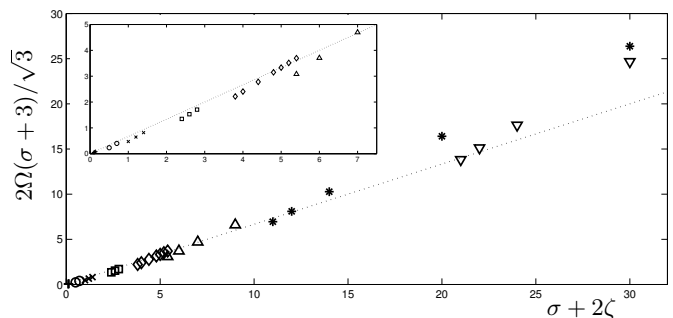


FIG. 4. The scaled spiral frequency $2\Omega(\sigma + 3)/\sqrt{3}$ plotted against $\sigma + 2\zeta$, for results from 2D simulations over a range of σ and ζ . The dotted line has a slope of $\frac{2}{3}$. The inset shows a zoom of the origin. Different symbols correspond to different values of σ : $(+, \circ, \times, \square, \diamond, \triangle, \star, \nabla)$.

almost $\frac{1}{3+\sigma}$, the value from the coexistence equilibrium. We therefore compared the rotation frequency Ω to the imaginary part of the complex eigenvalue at the coexistence equilibrium, plotting (in Fig. 4) $\frac{2}{\sqrt{3}}\Omega(\sigma + 3)$ against $\sigma + 2\zeta$, for spirals found over a wide range of values of σ and ζ . The data almost collapses on to a straight line of slope (approximately) $\frac{2}{3}$. If Ω were equal to the imaginary part of the complex eigenvalue, the slope would be 1.

This data collapse is sufficient to give a complete prediction for the properties of a spiral: Ω is set by the core and is approximately $\frac{2}{3}\frac{\sqrt{3}}{2}(\sigma + 2\zeta)/(3 + \sigma)$. The other two quantities γ and Λ are set by $\gamma = \Lambda/\Omega$ and the nonlinear dispersion relation in Fig. 2.

It remains to consider the far-field stability of the spirals. With $\sigma = 3.2$, we find 1000×1000 domain-filling 2D spirals (as in Fig. 1a) over the range $0.2 \leq \zeta \leq 1.2$. For values of ζ outside this range, the far field of the spiral breaks up (as in $\zeta = 2$ and 3 insets in Fig. 3), and for $\zeta = 0.2$ and $\zeta \geq 1.1$, this is also seen in a larger 2000×2000 domain. This pattern is repeated with other values of σ : in the range $0.1 \leq \sigma \leq 20$ (the limit of our exploration), we find stable domain-filling spirals with ζ no more than $\frac{\sigma}{2}$. For $\sigma \geq 2$ we also find a lower bound on ζ for such spirals, but for smaller σ and ζ , the wavelengths of the spirals (typically about $2\Lambda_H$) are so big that only two or three (or fewer) turns fit in to a 1000×1000 domain. The details of stability and its relation to domain size are worthy of further investigation [18].

An alternative approach to studying the effect of spatial structure on cyclic dominance introduces mutation between the three species, leading to a Hopf bifurcation from the coexistence equilibrium [7, 8]. Properties of small-amplitude (weakly nonlinear) spirals close to this Hopf bifurcation can be inferred by reducing (2) to a complex Ginzburg–Landau equation. Our approach treats the TW as fully nonlinear, close to a heteroclinic cycle, complementing the earlier work. Stability predic-

tions cannot be compared directly. True 2D spirals are in between these two extremes, but both approaches yield a $\sigma^{-\frac{1}{2}}$ scaling (for small σ) of the wavelength of the TWs.

The authors would like to thank Graham Donovan, Edgar Knobloch, Mauro Mobilia and Hinke Osinga for helpful discussions regarding this work. This work was started during a visit of CMP to Leeds partly funded by a Scheme 2 grant from the London Mathematical Society and the University of Auckland.

-
- [1] T. Reichenbach, M. Mobilia, and E. Frey, “Mobility promotes and jeopardizes biodiversity in rock-paper-scissors games,” *Nature* **448**, 1046–1049 (2007)
- [2] A. Szolnoki, M. Mobilia, L. Jiang, B. Szczesny, A. M. Rucklidge, and M. Perc, “Cyclic dominance in evolutionary games: a review,” *J. Roy. Soc. Interface* **11**, 20140735 (2014)
- [3] B. Kerr, M. A. Riley, M. W. Feldman, and B. J. M. Bohannan, “Local dispersal promotes biodiversity in a real-life game of rock-paper-scissors,” *Nature* **418**, 171–174 (2002)
- [4] B. Sinervo and C. M. Lively, “The rock-paper-scissors game and the evolution of alternative male strategies,” *Nature* **380**, 240–243 (1996)
- [5] B. Kerr, C. Neuhauser, B. J. M. Bohannan, and A. M. Dean, “Local migration promotes competitive restraint in a host-pathogen ‘tragedy of the commons’,” *Nature* **442**, 75–78 (2006)
- [6] E. Frey, “Evolutionary game theory: Theoretical concepts and applications to microbial communities,” *Physica A* **389**, 4265–4298 (2010)
- [7] B. Szczesny, M. Mobilia, and A. M. Rucklidge, “Characterization of spiraling patterns in spatial rock-paper-scissors games,” *Phys. Rev. E* **90**, 032704 (2014)
- [8] B. Szczesny, M. Mobilia, and A. M. Rucklidge, “When does cyclic dominance lead to stable spiral waves?,” *EPL* **102**, 28012 (2013)
- [9] R. M. May and W. J. Leonard, “Nonlinear aspects of competition between 3 species,” *SIAM J. Appl. Math* **29**, 243–253 (1975)
- [10] J. Guckenheimer and P. Holmes, “Structurally stable heteroclinic cycles,” *Math. Proc. Camb. Phil. Soc.* **103**, 189–192 (1988)
- [11] M. Krupa and I. Melbourne, “Asymptotic stability of heteroclinic cycles in systems with symmetry,” *Ergod. Theory Dyn. Syst.* **15**, 121–147 (1995)
- [12] K. Orihashi and Y. Aizawa, “Global aspects of turbulence induced by heteroclinic cycles in competitive diffusion Lotka-Volterra equation,” *Physica D* **240**, 1853–1862 (2011)
- [13] E. J. Doedel, R. C. Paffenroth, A. R. Champneys, T. F. Fairgrieve, Yu. A. Kuznetsov, B. Sandstede, and X. Wang, *AUTO 2000: Continuation and bifurcation software for ordinary differential equations (with HomCont)*, Tech. Rep. (Caltech, 2001)
- [14] A. Scheel and P. Chossat, “Bifurcation d’orbites périodiques à partir d’un cycle homocline symétrique,” *C. R. Acad. Sci. Paris Ser. I* **314**, 49–54 (1992)
- [15] A. R. Champneys, “Homoclinic orbits in reversible systems and their applications in mechanics, fluids and optics,” *Physica D* **112**, 158–186 (1998)
- [16] A. J. Homburg and B. Krauskopf, “Resonant homoclinic flip bifurcations,” *Journal of Dynamics and Differential Equations* **12**, 807–850 (2000)
- [17] S. M. Cox and P. C. Matthews, “Exponential time differencing for stiff systems,” *J. Comp. Phys.* **176**, 430–455 (2002)
- [18] M. Mobilia, A. M. Rucklidge, and B. Szczesny, “The influence of mobility rate on spiral waves in spatial rock-paper-scissors games,” *Games* **7**, 24 (2016), ISSN 2073-4336, <http://www.mdpi.com/2073-4336/7/3/24>